Running Head: Ignored marsh weakness to sea level rise

Vegetation recovery on neighboring tidal flats forms an Achilles' heel of saltmarsh resilience to sea level rise

Zhenchang Zhu[1,2*], Jim van Belzen[1†], Qin Zhu[2‡], Johan van de Koppel[§1] & Tjeerd J. Bouma[1,3**]

[1] Department of Estuarine and Delta Systems, Royal Netherlands Institute for Sea Research and Utrecht University, Yerseke 4400AC, The Netherlands

[2] Institute of Environmental and Ecological Engineering, Guangdong University of Technology, Guangzhou, China

[3] Faculty of Geosciences, Department of Physical Geography, Utrecht University, The Netherlands

[*] Corresponding author: zhenchang.zhu@nioz.nl,
[†] jim.van.belzen@nioz.nl
[‡] qin.zhu@nioz.nl
[§] johan.van.de.koppel@nioz.nl
[**] tjeerd.bouma@nioz.nl

22

23 **Key words:** vegetation recovery, resilience, sea level rise, wave, saltmarsh, tidal flat,
24 coastal protection

25

26

Abstract

Coastal wetlands such as saltmarshes are valued as prominent buffering ecosystems to global climate change and sea level rise (SLR), yet their long-term persistence may also be threatened by these global change stressors. While saltmarshes are increasingly thought to be resilient to SLR owing to high vertical marsh adaptability, their long-term stability remains uncertain due to our poor understanding of marsh resilience at the marsh-tidal flat interface, where wave disturbance can progressively shift vegetated marsh towards a bare tidal flat state. Here, we explore how SLR affects vegetation recoverability on tidal flats using cordgrass, a globally common saltmarsh foundation species, as a model plant. Combined field and model results demonstrate that small increases in wave forcing due to raised water depth over tidal flats can dramatically weaken or even block vegetation recovery from eroding marsh edges, through hampering seed persistence. Vegetation recovery on tidal flats next to the marsh edge thus represents an unrecognized Achilles' heel of marsh resilience to SLR, which if ignored may cause underestimation of marsh vulnerability. These findings are highly relevant for a more comprehensive assessment of marsh susceptibility to SLR in systems where seeds play an essential role in revegetation of tidal flats, and highlight the importance of maintaining either a wave-protected or well-elevated tidal flat near the marsh edge that allows for quick vegetation recovery for supporting resilient marshes.

Introduction

Coastal wetlands such as saltmarshes are among the most valuable ecosystems on the globe (Costanza et al. 1997), providing many key ecosystem functions such as carbon sequestration and flood protection (Barbier et al. 2011). These features render them prominent ecosystems that naturally buffer the impacts of global climate change as well as sea level rise (SLR) (Duarte et al. 2013; Temmerman et al. 2013). However, sea level rise also threatens the long-term persistence of coastal wetlands (Kirwan and Megonigal 2013; Wang et al. 2017) and in many cases its impacts are amplified by local land subsidence caused mainly by human activities (Syvitski et al. 2009). For over 30 years, there have been widespread concerns about marsh drowning in response to SLR, as this can shift extensive marsh area from the vegetated state to the bare tidal flat state (Kirwan and Megonigal 2013; Kirwan et al. 2016). A recent meta-analysis however concludes that - given sufficient sediment - the positive feedback between plant growth and enhanced sedimentation allows most marshes to compensate for SLR (Kirwan et al. 2016). This premise however ignores that many marshes face extensive erosion at the marsh edge (Deegan et al. 2012; Hughes et al. 2009; Leonardi et al. 2016; Silliman et al. 2012; van de Koppel et al. 2005), where plant-sediment feedbacks are rendered ineffective. Currently, the knowledge deficit on marsh adaptability in the lateral dimension severely limits our understanding of marsh resilience to SLR.

Lateral marsh losses occur when wave disturbance progressively shifts vegetated marsh towards a bare tidal flat state, often by means of cliff erosion (Allen 2000; Leonardi and Fagherazzi 2014; Marani et al. 2011; van der Wal and Pye 2004). Cliff erosion rate increases linearly with rising wave power and even very small waves may

cause erosion of large saltmarsh blocks (Leonardi and Fagherazzi 2014; Leonardi et al. 2016). A resilient marsh will display vegetation recovery and expansion on the tidal flats in front of the retreated marsh (Bouma et al. 2016; van de Koppel et al. 2005). Many meso- and macrotidal marshes have shown cyclic alternations between a marsh retreating phase and a vegetation recovery/expansion phase at the marsh-tidal flat interface on decadal or larger time scales (Allen 2000; Chauhan 2009; van der Wal et al. 2008). Both phases are influenced by wave-induced, erosive dynamics on the tidal flat next to the marsh edge (Bouma et al. 2016; Wang et al. 2017).

Unlike the highly adaptable marsh platform where plants trap sediment and reduce erosion (Kirwan and Megonigal 2013; Kirwan et al. 2016), the adjacent tidal flats are at high risk of becoming increasingly deep due to the rising sea level (Mariotti and Fagherazzi 2010), given the absence of positive plant-sedimentation feedback, the strong sediment competition between the marsh and adjacent tidal flats (Mariotti and Fagherazzi 2010) and worldwide declines of sediment delivery to coasts (Syvitski et al. 2009; Walling and Fang 2003). A numeric marsh-tidal flat co-evolution model predicts that, with low sediment availability, a small rate (2 mm/yr) of SLR may result in up to approximately 30 cm deeper tidal flats after 50 years, yet without causing significant drowning of adjacent vegetated marsh (Mariotti and Fagherazzi 2010). SLR-increased water depth on adjacent tidal flats allow stronger waves to reach the marsh edge (Arns et al. 2017; Mariotti and Fagherazzi 2010), as a result of reduced bottom friction and relaxed depth limitation. This can increase lateral erosion rates (Leonardi et al. 2016; Mariotti and Fagherazzi 2010; Wang et al. 2017), especially when biotic stressors e.g. crab burrowing and herbivory, etc. (Holdredge et al. 2009; Hughes et al. 2009) and human activities e.g. eutrophication and oil spilling, etc. (Deegan et al. 2012; Silliman et al. 2012) weaken erosion resistance at the marsh

edge. In this context, whether the marsh can persist in the long run and maintain adequate size for provisioning of key ecosystem services depends critically on a resilient marsh edge that is able to recover from phases of increased edge erosion. Yet, little is known about the consequence of SLR for marsh re-establishment on neighboring tidal flats following lateral retreat of the marsh edge. This knowledge gap significantly impedes comprehensive assessments of marsh susceptibility and accurate predictions of marsh fate under SLR.

Here, we bridge this knowledge gap by examining how SLR-intensified wave forcing shapes seed-based vegetation recovery on adjacent tidal flats (Fig. 1). Seedling establishment is a crucial process of vegetation recovery seen in many meso- and macrotidal marsh ecosystems around the world (Gray et al. 1991; Liu et al. 2017; Strong and Ayres 2013; Temmerman et al. 2007). Although marsh expansion is in some areas predominantly the result of clonal extension from the existing vegetation (e.g. Allison 1995; Angelini and Silliman 2012), seedling recruitment (Fig. 1b-f) often yields rapid vegetation establishment on tidal flats over extensive areas (Gray et al. 1991; Strong and Ayres 2013; Zhu et al. 2012). Seed-based establishment appears to be especially important in meso- and macro- tidal systems where clonal expansion can be halted by the formation of a high cliff at the marsh edge (Fig. 1c), which completely disconnects the tidal flats from the existing vegetation. However, seedling establishment is often constrained by wave disturbance and associated sediment erosion that imposes difficulties for seed persistence (Groenendijk 1986; Marion and Orth 2012; Zhu et al. 2014) and seedling survival (Balke et al. 2013; Bouma et al. 2009; Bouma et al. 2016; Friess et al. 2012). Therefore, we hypothesize that SLR-increased wave forcing may undermine marsh resilience at the seaward edge of the marsh where seed colonization is a critical pathway for vegetation recovery.

To test our hypothesis, we combined field measurements and model simulations to quantify the impacts of shifting wave forcing on the ability of the marsh to recover by seed establishment when it has shifted to an unvegetated tidal flat state, using cordgrass (*Spartina* Spp.) as a model. Cordgrass globally defines and stabilizes shorelines, laying the foundation for saltmarshes to develop (Strong and Ayres 2013), and seeds often play a critical role in its establishment and range expansion in many parts of the world (Ayres et al. 2008; Gray et al. 1991; Xiao et al. 2009). Seed availability is the prerequisite for seedling establishment on tidal flats and hydrodynamic-induced seed removal from the tidal flat surface is a major source of seed loss (Groenendijk 1986; Marion and Orth 2012; Zhu et al. 2014). Hence, we first determined the response of surface seed retention to increasing wave actions by conducting large-scale experiments in field locations with varying wave forcing in a NW Delta, the Scheldt estuary (Fig. 2a). Based on this relationship, we next develop a spatial model to assess the consequences of SLR intensified wave forcing for seed-based vegetation recoverability.

Materials and Methods

Quantifying the response of seed retention to varying wave forcing on tidal flats

Study sites and species

The Scheldt estuary is a macrotidal estuary situated near the border between the Netherlands and Belgium. The mean tidal range increases from 3.8 m near the mouth of the estuary to >5.0 m upstream of the border (Baeyens et al. 1998). It was originally composed of two aligned and interconnected water bodies called Westerschelde and Oosterschelde. Due to land reclamation in 1860s, the

145 Oosterschelde was progressively separated from the Westerschelde. The pioneer salt
146 marsh vegetation in the meso- and polyhaline (> 5 ppt) part of the estuary consists
147 mainly of the perennial common cordgrass (*Spartina anglica*), which was introduced
148 to the Scheldt estuary in the 1920s (Groenendijk 1986; van der Wal et al. 2008).

149 Cordgrass can produce a large amount of seeds, although there is high variability
150 between years and locations (Gray et al. 1991; Strong and Ayres 2013; Xiao et al.
151 2009). Because of the short (less than 1 year) seed longevity (Wolters and Bakker
152 2002; Xiao et al. 2009), seedling establishment of cordgrass on tidal flats requires
153 annually built seed banks as a result of seed delivery from the marsh by the tide
154 (Huiskes et al. 1995; Zhu et al. 2014). Although the minimal period that such transient
155 seed banks need to persist is short, i.e., the period between when seeds become
156 available (autumn) and seedlings start to emerge (spring), the persistence during this
157 short period is vital for the occurrence of seedling recruitment (Groenendijk 1986;
158 Zhu et al. 2014). Seed dislodgement by waves and associated sediment erosion is a
159 major source of seed loss from the tidal flat; seeds are especially vulnerable when
160 they are on the surface (Groenendijk 1986; Zhu et al. 2014).

161 *Quantifying seed retention under varying wave conditions*

162 To quantify the relationship between surface seed retention and wave forcing, we
163 selected 8 field locations (tidal flats near a marsh) in the Scheldt estuary with varying
164 water depth (Fig. 2a, table. 1), including both relatively wind sheltered and exposed
165 sites (Callaghan et al. 2010; Suykerbuyk et al. 2016). The study locations include
166 seven mudflats near the marsh in the Scheldt estuary (Fig. 2a) with different wind
167 exposure (Callaghan et al., 2010, Suykerbuyk et al., 2016) ; The elevation of the
168 experimental area was ca. 90 cm above NAP (i.e., Dutch ordinance level, close to

mean sea level) for most field sites, while a higher elevation (175 cm NAP) was chosen for two Westerschelde sites: ZG & BA where salt marshes are less deep. At ZG, we included an additional location with a lower elevation (ca. 90 cm NAP).

Our experiments and measurements were implemented during the relatively storm-free period, April-July (T0-T4, electronic supplementary material, table. S1) to obtain a range of wave conditions including both small and large waves. At each location, we quantified the retention of surface seeds by seed sowing and recovery experiments. We conducted three trials at each site with a duration of 4 weeks (trial1: T0-T1; trial2: T1-T2) and 2 weeks (trial3: T3-T4). In each trial, five 20 x 20 cm quadrats were laid in a row at 1m intervals. Within each quadrat, 50 cordgrass seeds were randomly sowed on the sediment surface. These quadrats were positioned along a 6 m-long string (marked every 1 m) with each end fixed at a PVC tube. The sowed seeds were first sterilized by freezing them in a –20 °C freezer for two weeks to prevent seed loss due to germination (Zhu et al. 2016). These seeds were then dyed with Rose Bengal to be distinguished from the ambient seeds and were waterlogged to mimic the naturally settled cordgrass seeds (Zhu et al. 2014).

Upon recovery, sediment bulks (each 40 x 40 x 5 cm, Length x Width x Depth) were excavated after relocation of the quadrates using the same string. There was no seed visible on the surface when recovered. We sampled the top 5 cm to recover the seeds that may have been buried. The recovered area was chosen to be twice as big as the seed-deployment area, to account for the seeds that might have merely moved to the close vicinity. Seeds not recovered within this area were regarded as ‘lost’. The retrieved sediment was transported back to the lab and sieved through a 0.1 cm sieve, to quantify the remaining seeds. Seed retention (%) during each trial period was

193 calculated as recovered/deployed and averaged among the five replicates at each
194 location.

195 *Quantifying wave forcing in relation to seed retention*

196 The wave forcing and tidal level of each location was measured in 2013 during T0-T4
197 (Table. S1), using pressure sensors (OSSI-010-003C; Ocean Sensor Systems, Inc.)
198 deployed in the experiment zone. Every wave gauge was mounted on a pole inserted
199 into the soil about 1 m deep. Each sensor was approximately 5 cm above the tidal flat
200 surface. The measuring interval and period were 15 minutes and 7 minutes,
201 respectively. The wave analysis was based on pressure fluctuations, measured with a
202 frequency of 5 Hz. The recorded pressure readings were converted to water level
203 fluctuations, which were then corrected by removing erroneous spikes, shifts,
204 corrupted bursts and low frequency tidal components (Callaghan et al. 2010;
205 Christianen et al. 2013). From the detrended data, wave parameters including
206 significant wave height (H_s) and peak wave period (T_p) were calculated based on the
207 linear wave theory (Tucker and Pitt 2001).

208 Wave-induced shear stress ($\tau_{wave,}$ Pa) on the sediment surface is a relevant measure for
209 the hydrodynamic energy in relation with sediment motion (Callaghan et al. 2010),
210 making it a good proxy for the wave forcing that dislodge seeds on the surface. τ_{wave} is
211 calculated as follows (van Rijn 1993):

212 $$\tau_{wave} = \frac{1}{4}\rho_w f_w \hat{U}_\delta^2$$

213 where ρ_w is the sea water density (kg/m3), $\hat{U}_\delta$ is near-bed orbital velocity, calculated
214 as:

215 $$\hat{U}_\delta = \frac{\pi H}{T \sinh(kh)}$$

216 in which H is wave height (m), T is wave period (s), k is wave number (m^{-1}),
217 calculated by solving $(2\pi/T)^2 = gk\tanh(kh)$ (Swart 1977), and h is water depth (m).
218 In practice, significant wave height H_s and peak wave period T_p are used as H and T
219 in the formulae.

220 The wave friction coefficient (-) f_w is determined by the following equation (Swart
221 1977):

222 $$f_w = \min\left\{\exp\left[-6 + 5.2\left(\frac{\hat{A}_\delta}{2.5\, d_{50}}\right)^{-0.19}\right], 0.3\right\}$$

223 where the peak orbital excursion $\hat{A}_\delta$ is expressed as $\hat{A}_\delta = \frac{H}{2\sinh(kh)}$, d_{50} is median grain
224 size of the bed sediment (m).

225 A breaking-wave check was carried out before the τ_{wave} calculation, as the theory
226 mentioned above is applied to non-breaking waves. In our cases, wave heights over
227 water depths (H_s/h) were all less than 0.78, indicating local non-breaking condition
228 (Kaminsky and Kraus 1993).

229 For each location, we determined the time-averaged wave-imposed shear stress
230 (τ_{wave_avg}) on the tidal flat surface to measure the overall wave disturbance to the
231 surface seeds. τ_{wave_avg} was determined for 4 monitoring period T0-T1, T1-T2, T2-T3
232 and T3-T4, respectively (Table. S1). For each period, we also determined maximum
233 significant wave height (H_{s_max}), water depth ($h_{\_max}$) and inundation frequency.

234

Measurement of bed level change

Additionally, the elevation in the experimental zone of each location was monitored monthly using a 3D Laser scanner (RIEGL VZ-400) to detect the patterns of bed level change of each location. All the scans were georeferenced with the Riscan program that came with the scanner. The scans were clipped to the experiment zone. The resulting points were exported to an LAS-file that was later imported to ArcGis10. For each 5 x 5 cm the maximum value is used to produce a raster. To partly fill the holes in the raster the maximum value for each 20 x 20 cm was also adopted. The two rasters were mosaicked, 5 cm on top. For each location, 20 random points from an undisturbed area (ca. 75 x 75 cm) in each plot and the undisturbed area in between plots were selected, respectively, to calculate the mean elevation at each time point. The scanning was conducted at T0, T1, T2 and T5 (Table. S1). Due to the instrument failure, elevation values were not available at T2 for DO, RA & ZA.

Statistics

Data from all field locations were pooled together for statistics. We used Pearson's correlation to analyze the relationship between seed retention and τ_{wave_avg}. Prior to the analysis, data normality was checked through Shapiro‐Wilk tests. The seed retention was square root transformed to satisfy the requirement of data normality. After a significant correlation between seed retention and τ_{wave_avg} was found, we applied different types of curve fits (including both linear and non-linear) to find a regression equation that can best explain the relationship between these two variables. All the statistical analyses were done in R (http://www.R-project.org), applying a significance level of $\alpha = 0.05$.

Modeling the impacts of intensified wave forcing on revegetation of tidal flats

We developed a cellular automation-based model to assess the consequences of SLR-intensified wave forcing for seed-based marsh recoverability on neighboring tidal flats. The model domain consists of a matrix of 1000*1000 cells, which represent a landscape of 100 * 100 m with each cell 0.1*0.1 m. In this model, revegetation of tidal flats starts with seedling recruitment, which serves as nuclei for subsequent vegetative growth (Fig. 1 e-g). For each cell, there are three possible states: bare state, seedling state or vegetated state. The model starts with a landscape consisted of bare cells. A bare cell first shifts to a seedling cell when seedling recruitment occurs, and later becomes a vegetated cell at the end of each year (time step). A bare cell can also directly change into a vegetated cell by vegetative growth when there are vegetated cells in the neighborhood.

The number of cells that transfer from the 'bare' state to 'seedling' state increases with seedling density (no. /m^2). Seedling density is set to decrease with increasing distance to the marsh edge with its peak occurring near the marsh edge, complying with observed patterns in the field (Xiao et al. 2010; Zhu et al. 2012). Peak seedling density (D_{peak}) is determined by two parameters: *i)* the wave-imposed shear stress on the tidal flat surface (τ_{wave_avg}, Pa), the primary factor limiting seedling density by minimizing seed retention on tidal flats; and *ii)* a seedling abundance coefficient (*Sc*), reflecting the lumped effects of all factors other than waves on seedling recruitment, such as seed availability, seed germination and seedling-mortality caused by various factors e.g. sediment erosion (Bouma et al. 2016; Cao et al.), bioturbation (van Wesenbeeck et al. 2007), herbivory (Paramor and Hughes 2004; Zhu et al. 2016), etc. A lower value of *Sc* means stronger inhibition on seedling recruitment from these

282 factors and vice versa.

283 D_{peak} is calculated by the following equation:

284 $$D_{peak} = Sc * e^{-102.6 * \tau_{wave\_avg}}$$

285 Seedling density at a given distance is calculated as:

286 $$D_s = D_{peak} * Ks/(Ks+ds)$$

287 where *ds* (an integer between 1 and 1000) is the distance to the marsh edge and *Ks* is
288 the half saturation constant for *ds*. Since the decay rate of seed delivery and seedling
289 survival with increasing distance to the marsh edge can be highly site-specific, we
290 made *Ks* a random integer between 10 (1 m) and 250 (25 m). We applied this
291 maximum value based on the field data from a Chinese marsh with the ever-reported
292 fastest cordgrass expansion by seedling recruitment (Xiao et al. 2010; Zhu et al. 2012).

293 The number of seedling cells at a given distance is determined as:

294 $$n_s = \min (D_s * n * A, n)$$

295 where *n* is the number of cells at that distance, *A* is the area of each cell (i.e. 0.01 m^2).
296 The positions of the seedling cells at a given distance were randomly determined.

297 To account for stochastic disasters such as severe storms that may wipe out all the
298 seeds or established seedlings, the model randomly decides whether a given year is a
299 bad year. When it is a 'bad year', seedling cells turn back to bare cells at the end of
300 the year, whereas seedling cells become vegetated cells at the end of each good year.

301 The transition probability from a bare cell to a vegetated cell by clonal growth is
302 determined by the number of neighboring vegetated cells. The neighborhood size is

303 determined by clonal growth rate. Since clonal growth rate of cordgrass was found to
304 be highly variable and usually less than 2 m (i.e. 20 cells) per year (Gray et al. 1991;
305 Xiao et al. 2010; Zhu et al. 2012), we adopted a random integer between 1 and 20 for
306 clonal growth rate (cells/yr) for each time step.

307 We conducted numeric experiments by varying both the values of wave-imposed
308 shear stress on the tidal flat surface τ_{wave_avg} and the seedling abundance coefficient *Sc*.
309 For τ_{wave_avg}, we applied a wide range of values from 0.01 to 0.08 Pa (based on field
310 observation, Fig. 2d) with an interval of 0.0025 Pa, and we adopted three distinct
311 values (0.01, 0.1 and 1) for *Sc* to reproduce seedling densities that cover the natural
312 range for cordgrass seedlings observed in the field (Gray et al. 1991; Liu et al. 2017;
313 Xiao et al. 2010; Zhu et al. 2012). For each combination of τ_{wave_avg} and *Sc*, we first
314 sort out the scenarios when seed colonization is completely disabled. Where seedling
315 establishment is possible, we run the model 100 times, and for each run we
316 determined the recovery time i.e. the number of years it takes to recover the given 100
317 *100 m landscape. The landscape is considered as 'recovered' when 90% of the cells
318 become vegetated. After these initial runs, we added three sets of scenarios to detect
319 the sensitivity of recovery time to small increments of wave heights. For each set of
320 scenario, we raised τ_{wave_avg} by 0.001, 0.002 and 0.003 Pa, respectively, which
321 corresponds to approximately 1, 2 and 3 cm rise of maximum significant wave height,
322 respectively, according to the empirical relationship derived from our field
323 measurements (Fig. 2d). We ran each scenario 100 times and determined the recovery
324 time, which was then averaged and compared to the initial recovery time to detect
325 how raised wave heights cause changes in marsh vegetation recoverability on tidal
326 flats.

Results

Effects of increasing wave disturbance on seed retention on tidal flats

The field results showed that the persistence of the seeds on the tidal flat surface decayed exponentially with increasing wave disturbance (Fig. 2b), measured as the time-averaged shear stress that the waves imposed on the tidal flat surface (τ_{wave_avg}). This relation is significant (Pearson's correlation, $p < 0.01$) when excluding the only outlier (i.e. the extremely high value) observed at ZG_{LOW} (Fig. 2b). ZG_{LOW} is the sole location characterized by continuously fast sediment accretion (ca. 1.2 mm/d, Fig. S1), which most likely result from the dumping of dredged sediment near this location (Sistermans and Nieuwenhuis 2019). This may explain the outlier, as fast sediment accretion might occasionally offer the seeds a window of opportunity to get sufficiently buried to escape subsequent wave disturbance on surface seed. Such burial-scenario is however expected to be rare, given the rarity of fast accretion in autumn, winter and early spring (Andersen et al. 2006; Hu et al. 2017; Yang et al. 2008; Zhu et al. 2012), during which cordgrass seeds are dispersed (Huiskes et al. 1995; Xiao et al. 2009). When excluding all the data points (n=3 for ZG_{LOW} and n=1 for BA) associated with fast sediment accretion (> 1 mm/d, Fig. S1), the relationship between seed retention and τ_{wave_avg} remains significant (Pearson's correlation, $p < 0.01$, Fig. S2) with a comparable declining trend as shown in Fig.2b.

Field measurements reveal a clear positive effect of water depth on wave strength; supporting the assumption that SLR-increased water depth on tidal flats intensifies wave forcing. Increased water depth allows higher maximum significant wave heights (Fig. 2c), which is proportional to mean significant wave heights (Fig. S3). Increased maximum significant wave heights, plus a longer inundation period due to raised

water depths, results in stronger shear stress wave imposed on the tidal flat surface (Fig. 2d). For a given water depth, the relatively wave exposed sites have higher wave heights than the relatively wave sheltered sites (Fig. 2c), indicating that SLR impacts on wave forcing may be amplified if climate change leads to stronger or more frequent winds towards the coasts.

Modeling the impacts of intensified wave forcing on marsh revegetation

The model reveals the same vegetation expansion dynamics as observed in the field: seedling establishment yields satellite clumps, which then extend laterally and eventually merge into continuous meadows through clonal growth (Fig. 3). The number of established seedlings thus strongly controls the speed of vegetation expansion on the tidal flats (Fig. 3). Hence, mean revegetation rate increases non-linearly with increasing peak seedling density, but it becomes more or less constant once the peak seedling density (no. /m2) becomes higher than 10 (Fig. 4a). Peak seedling density declines non-linearly with time-averaged wave-induced bed shear stress (τ_{wave_avg}), with its magnitude regulated by the seedling abundance coefficient (Fig. 4b).

Generally, under nominal conditions, our model produced comparable revegetation rates as observed in the field. For example, a 100 m long (cross-shore) tidal flat was predicted to be vegetated with an average expansion rate of 28 m/yr for a peak seedling density of ca. 6 no./m^2 (Fig. 4a), which parallels the observed rapid cordgrass expansion in a Chinese marsh with comparable seedling densities: 25 m in 2009 (Xiao et al. 2010) and 39 m in 2010 (Zhu et al. 2012). Moreover, field observations in saltmarshes in East Asia (Cao et al. ; Liu et al. 2017; Xiao et al. 2010; Zhu et al. 2012), NW Europe (Bouma et al. 2016; Gray et al. 1991; Nehring and Hesse 2008) and the

375 Pacific coast of US (Ayres et al. 2004; Strong and Ayres 2013) confirm our model
376 predictions that seedling recruitment allows for much faster vegetation establishment
377 than what would be observed when clonal growth from the existing marsh edge is the
378 only driving process (Fig. 4a).

379 The model results (Fig. 5a) clearly show that vegetation recovery time grows non-
380 linearly with increasing wave-imposed shear stress on the tidal flat surface (τ_{wave_avg})
381 until seed colonization is completely disabled. The sensitivity of the recovery rate to
382 rising τ_{wave_avg} decreases with increased value of seedling abundance coefficient (i.e.
383 reduced negative effects from other stressors), while it increases with declined
384 seedling density. For instance, increased τ_{wave_avg} does not affect recovery rate much
385 when peak seedling density is higher than 0.4 no./m^2, whereas it greatly slows down
386 and eventually disables seed-based revegetation when peak seedling density is
387 between 0 and 0.4 no./m^2 (Fig. 5a).

388 Further analyses reveal that a small increase of wave height on tidal flats due to SLR-
389 increased water depth can considerably lengthen marsh recovery time, especially
390 when the initial recovery is already slow (Fig. 5b). For instance, with a low initial
391 recoverability (recovery time = 47 yr), a 3 cm rise of maximum significant wave
392 height (H_{s_max}) nearly doubles the recovery time and even only a 1 cm increase of
393 H_{s_max} lengthens the recovery time by approximately 25 % (Fig. 5b). In the field
394 locations used in this study, 1 cm rise of maximum significant wave height can be
395 achieved by an increase of maximum water depth between 2.5 cm and 8.3 cm,
396 depending on wave exposure (Fig. 2c).

Discussion

The current study highlights that saltmarshes are more vulnerable to SLR than previously considered. Our results reveal high sensitivity of seed-based revegetation of bare tidal flats to intensified wave forcing that non-linearly lengthens the vegetation recovery time. A small increase of water depth on the tidal flat resulting from SLR is able to cause a major decline in lateral marsh recoverability (i.e. marsh resilience to lateral erosion) by lowering seed persistence. Hence, revegetation of tidal flats next to the marsh edge forms an Achilles' heel of saltmarsh resilience to SLR in systems where vegetation recovery typically starts from seeds, as seen in many meso- and macro- tidal systems (Gray et al. 1991; Liu et al. 2017; Strong and Ayres 2013; Temmerman et al. 2007). While recent literature highlights that the risk of saltmarsh drowning in response to sea level rise has been overstated as marshes are able to adapt when sediment availability is sufficient (Kirwan et al. 2016), the current study demonstrates that SLR can significantly weaken marsh resilience at the seaward boundary by hampering vegetation recovery from seeds at the seaward edge of an eroding marsh.

In addition to the primary findings, the results also suggest that SLR impacts on seed-based marsh recovery may be magnified by other stressors such as bioturbation (van Wesenbeeck et al. 2007) and herbivory (Paramor and Hughes 2004; Zhu et al. 2016) that can inhibit seedling recruitment. Enhanced negative effects (i.e. lower seedling abundance coefficient) from such stressors increase the sensitivity of the marsh recovery process to changing wave forcing (Fig. 3a). In addition, despite the revealed strong impacts of waves on seed-based revegetation, the present assessment is likely to be underestimated, as we only looked at seed removal and did not consider the

421 negative effects of wave disturbance on seedling survival (Bouma et al. 2016). In
422 reality, seed-based vegetation recovery of cordgrass on neighboring tidal flats may be
423 more susceptible to SLR increased wave forcing than what we showed in the model.

424 Given raised lateral marsh erosion risks under SLR as shown in earlier studies
425 (Leonardi et al. 2016; Mariotti and Fagherazzi 2010; Wang et al. 2017), declined
426 vegetation recoverability on adjacent tidal flats may over time result in a near-
427 irreversible lateral marsh collapse, due to increased wave exposure resulting from
428 raised water depths (Arns et al. 2017, this study; Mariotti and Fagherazzi 2010).
429 Although vertical marsh adaptability eases the risk of coastal squeeze (Pontee 2013),
430 i.e. reduced marsh width due to SLR-induced drowning along with prevented
431 landward migration by seawalls (or otherwise called dikes, levees etc.), our study
432 highlights that marshes in front of seawalls still can suffer significant habitat loss due
433 to declined lateral marsh recoverability to lateral erosion. This can impair the value of
434 key ecosystem services of saltmarshes such as flood protection which depends
435 critically on ecosystem size (Bouma et al. 2014), especially for marshes that have
436 already declined in area due to land reclamation (Kirwan and Megonigal 2013).

437 The current paper underscores the importance of maintaining a cascade protection of
438 ecosystems for supporting resilient coasts. Habitats at lower tidal elevations (i.e. the
439 bare tidal flat) that do not make a direct contribution for flood defense can influence
440 the resilience and long-term persistence of ecosystems at higher tidal elevations (e.g.,
441 saltmarshes) that directly protect the coast against flooding (Bouma et al. 2014;
442 Mariotti and Fagherazzi 2013). Maintaining sustainable nature-based coastal defenses
443 by saltmarshes in the face of sea level rise thus entails not only an adaptable marsh
444 platform, but also ensuring protection of the neighboring tidal flats that allows for

resilient marshes. Hence, management policies should enforce a cascade of protection: maintain well-elevated or wave-protecting tidal flats to sustain resilient marshes and thus safer coasts. This may be achieved by supply of dredging materials (Mendelssohn and Kuhn 2003; Temmerman et al. 2013) to reach a sufficiently high accretion rate that allows the tidal flat to adapt to SLR or by restoring shellfish reef ecosystems that limit wave formation on the tidal flat (Scyphers et al. 2011; Temmerman et al. 2013).

The present research underpins recent suggestions to manage ecosystem connectivity in order to preserve coastal ecosystems (Gillis et al. 2014; Gillis et al. 2017). Moreover, we demonstrate how such an approach becomes increasingly important in the face of global change. Beyond saltmarshes and adjacent tidal flats, other connected ecosystems may also display a cascade of vulnerability to environmental changes. For instance, in tropical coastal ecosystems, habitat losses of wave-damping coral reefs or seagrass beds due to climate change or human disturbances risk weakened stability of the neighboring mangrove forests (Gillis et al. 2014; Gillis et al. 2017). Similarly, the resilience of upland Amazon forests is likely to be impaired by the adjacent floodplains, which are more prone to the shift into a fire-dominated savanna state when the Amazon region becomes drier under climate change (Flores et al. 2017). Hence, we argue that the cascading protection strategy may be commonly needed to enhance the overall resilience of important landscapes or seascapes, constituted by spatially and functionally connected ecosystems, to the changing environment.

To conclude, we reveal saltmarsh recovery on the neighboring tidal flat habitats as an unrecognized Achilles' heel of saltmarsh resilience to sea level rise. The present

findings are highly relevant for a more comprehensive assessment of marsh susceptibility to sea level rise and more accurate predictions of long-term dynamics of marshes where seeds play a critical role in vegetation recruitment. While coastal wetlands such as saltmarshes are increasingly proposed to act as climate-change buffers to enhance the resilience of coastal communities (Bouma et al. 2014; Duarte et al. 2013; Temmerman et al. 2013), our study suggests that human intervention would be duly needed to improve the resilience of these buffering ecosystems as well as their protecting neighbors to warrant a sustainable, nature-based, coastal adaptation to global climate change.

Data accessibility. The code of the model and the field data of waves and seed retention that support the findings of this study are available in 4TU.ResearchData: https://doi.org/10.4121/uuid:c160edca-6234-439b-8600-5c6f7d81b46e.

Competing interests. We have no competing interests

Funding. Z.Z. and T.J.B. were funded by the BE-SAFE project (grant#: 850.13.011) financed by the Netherlands Organization for Scientific Research (NWO). Z.Z. was also supported by the project funded by China Postdoctoral Science Foundation (2019M652825). J.v.B. and J.v.d.K. were supported by the VNSC project "Vegetation modeling HPP"(contract 3109 1805).

Acknowledgement:

We are grateful to Lennart van IJzerloo, Jeroen van Dalen, Nanyang Chu, Artis Vansovics for their assistances in the field. We also thank Valarie de Witte for her help in checking the grammar.

References:

Allen, J. R. 2000. Morphodynamics of Holocene salt marshes: a review sketch from the Atlantic and Southern North Sea coasts of Europe. Quaternary Science Reviews **19:** 1155-1231.

Allison, S. K. 1995. Recovery From Small‐Scale Anthropogenic Disturbances by Northern California Salt Marsh Plant Assemblages. Ecological Applications **5:** 693-702.

Andersen, T. J., M. Pejrup, and A. A. Nielsen. 2006. Long-term and high-resolution measurements of bed level changes in a temperate, microtidal coastal lagoon. Mar Geol **226:** 115-125.

Angelini, C., and B. R. Silliman. 2012. Patch size-dependent community recovery after massive disturbance. Ecology **93:** 101-110.

Arns, A., S. Dangendorf, J. Jensen, S. Talke, J. Bender, and C. Pattiaratchi. 2017. Sea-level rise induced amplification of coastal protection design heights. Scientific Reports **7**.

Ayres, D. R., D. L. Smith, K. Zaremba, S. Klohr, and D. R. Strong. 2004. Spread of exotic cordgrasses and hybrids (*Spartina sp*.) in the tidal marshes of San Francisco Bay, California, USA. Biological Invasions **6:** 221-231.

Ayres, D. R., K. Zaremba, C. M. Sloop, and D. R. Strong. 2008. Sexual reproduction of cordgrass hybrids (Spartina foliosa x alterniflora) invading tidal marshes in San Francisco Bay. Diversity and Distributions **14:** 187-195.

Baeyens, W., B. van Eck, C. Lambert, R. Wollast, and L. Goeyens. 1998. General description of the Scheldt estuary. Hydrobiologia **366:** 1-14.

Balke, T., E. L. Webb, E. van den Elzen, D. Galli, P. M. J. Herman, and T. J. Bouma. 2013. Seedling establishment in a dynamic sedimentary environment: a conceptual framework using mangroves. Journal of Applied Ecology **50:** 740-747.

Barbier, E. B., S. D. Hacker, C. Kennedy, E. W. Koch, A. C. Stier, and B. R. Silliman. 2011. The value of estuarine and coastal ecosystem services. Ecological Monographs **81:** 169-193.

523 Bouma, T. J. and others 2009. Effects of shoot stiffness, shoot size and current
524 velocity on scouring sediment from around seedlings and propagules. Marine
525 Ecology Progress Series **388:** 293-297.

526 Bouma, T. J. and others 2016. Short-term mudflat dynamics drive long-term cyclic
527 salt marsh dynamics. Limnology and Oceanography **61:** 2261-2275.

528 Bouma, T. J. and others 2014. Identifying knowledge gaps hampering application of
529 intertidal habitats in coastal protection: Opportunities & steps to take. Coastal
530 Engineering **87:** 147-157.

531 Callaghan, D. P., T. J. Bouma, P. Klaassen, D. van der Wal, M. J. F. Stive, and P. M.
532 J. Herman. 2010. Hydrodynamic forcing on salt-marsh development:
533 Distinguishing the relative importance of waves and tidal flows. Estuarine
534 Coastal and Shelf Science **89:** 73-88.

535 Cao, H., Z. Zhu, T. Balke, L. Zhang, and T. J. Bouma. Effects of sediment
536 disturbance regimes on Spartina seedling establishment: Implications for salt
537 marsh creation and restoration. Limnology and Oceanography**:** n/a-n/a.

538 Chauhan, P. P. S. 2009. Autocyclic erosion in tidal marshes. Geomorphology **110:**
539 45-57.

540 Christianen, M. J. A. and others 2013. Low-Canopy Seagrass Beds Still Provide
541 Important Coastal Protection Services. Plos One **8:** e62413.

542 Costanza, R. and others 1997. The value of the world's ecosystem services and
543 natural capital. Nature **387:** 253.

544 Deegan, L. A. and others 2012. Coastal eutrophication as a driver of salt marsh loss.
545 Nature **490:** 388-392.

546 Duarte, C. M., I. J. Losada, I. E. Hendriks, I. Mazarrasa, and N. Marbà. 2013. The
547 role of coastal plant communities for climate change mitigation and adaptation.
548 Nature Climate Change **3:** 961-968.

549 Flores, B. M. and others 2017. Floodplains as an Achilles' heel of Amazonian forest
550 resilience. Proceedings of the National Academy of Sciences **114:** 4442-4446.

551 Friess, D. A. and others 2012. Are all intertidal wetlands naturally created equal?
552 Bottlenecks, thresholds and knowledge gaps to mangrove and saltmarsh
553 ecosystems. Biological Reviews **87:** 346-366.

554 Gillis, L. and others 2014. Potential for landscape-scale positive interactions among
555 tropical marine ecosystems.

556 Gillis, L. G., C. Jones, A. Ziegler, D. van der Wal, A. Breckwoldt, and T. Bouma.
557 2017. Opportunities for Protecting and Restoring Tropical Coastal Ecosystems
558 by Utilizing a Physical Connectivity Approach. Frontiers in Marine Science **4:**
559 374.

560 Gray, A. J., D. F. Marshall, and A. F. Raybould. 1991. A century of evolution in
561 *Spartina anglica*. Advances in Ecological Research **21:** 1-62.

562 Groenendijk, A. M. 1986. Establishment of a *Spartina-anglica* population on a tidal
563 mudflat - A field experiment. Journal of Environmental Management **22:** 1-12.

564 Holdredge, C., M. D. Bertness, and A. H. Altieri. 2009. Role of Crab Herbivory in
565 Die-Off of New England Salt Marshes. Conservation Biology **23:** 672-679.

566 Hu, Z., P. Yao, D. van der Wal, and T. J. Bouma. 2017. Patterns and drivers of daily
567 bed-level dynamics on two tidal flats with contrasting wave exposure.
568 Scientific Reports **7:** 7088.

569 Hughes, Z. J., D. M. FitzGerald, C. A. Wilson, S. C. Pennings, K. Więski, and A.
570 Mahadevan. 2009. Rapid headward erosion of marsh creeks in response to
571 relative sea level rise. Geophysical Research Letters **36**.

572 Huiskes, A. H. L., B. P. Koutstaal, P. M. J. Herman, W. G. Beeftink, M. M. Markusse,
573 and W. D. Munck. 1995. Seed dispersal of halophytes in tidal salt marshes.
574 Journal of Ecology **83:** 559-567.

575 Kaminsky, G. M., and N. C. Kraus. 1993. Evaluation of depth-limited wave breaking
576 criteria, p. 180-193. Ocean Wave Measurement and Analysis (1993). ASCE.

577 Kirwan, M. L., and J. P. Megonigal. 2013. Tidal wetland stability in the face of
578 human impacts and sea-level rise. Nature **504:** 53-60.

579 Kirwan, M. L., S. Temmerman, E. E. Skeehan, G. R. Guntenspergen, and S.
580 Fagherazzi. 2016. Overestimation of marsh vulnerability to sea level rise.
581 Nature Climate Change **6:** 253-260.

582 Leonardi, N., and S. Fagherazzi. 2014. How waves shape salt marshes. Geology **42:**
583 887-890.

584 Leonardi, N., N. K. Ganju, and S. Fagherazzi. 2016. A linear relationship between
585 wave power and erosion determines salt-marsh resilience to violent storms and
586 hurricanes. Proceedings of the National Academy of Sciences **113:** 64-68.

587 Liu, W., D. R. Strong, S. C. Pennings, and Y. Zhang. 2017. Provenance‐by‐
588 environment interaction of reproductive traits in the invasion of Spartina
589 alterniflora in China. Ecology.

590 Marani, M., A. D'Alpaos, S. Lanzoni, and M. Santalucia. 2011. Understanding and
591 predicting wave erosion of marsh edges. Geophysical Research Letters **38**.

592 Marion, S. R., and R. J. Orth. 2012. Seedling establishment in eelgrass: seed burial
593 effects on winter losses of developing seedlings. Marine Ecology Progress
594 Series **448:** 197-207.

595 Mariotti, G., and S. Fagherazzi. 2010. A numerical model for the coupled long‐term
596 evolution of salt marshes and tidal flats. Journal of Geophysical Research:
597 Earth Surface **115**.

598 Mariotti, G., and S. Fagherazzi. 2013. Critical width of tidal flats triggers marsh
599 collapse in the absence of sea-level rise. Proceedings of the national Academy
600 of Sciences **110:** 5353-5356.

601 Mendelssohn, I. A., and N. L. Kuhn. 2003. Sediment subsidy: effects on soil–plant
602 responses in a rapidly submerging coastal salt marsh. Ecological Engineering
603 **21:** 115-128.

604 Nehring, S., and K.-J. Hesse. 2008. Invasive alien plants in marine protected areas:
605 the *Spartina anglica* affair in the European Wadden Sea. Biological Invasions
606 **10:** 937-950.

607 Paramor, O. A. L., and R. G. Hughes. 2004. The effects of bioturbation and herbivory
608 by the polychaete *Nereis diversicolor* on loss of saltmarsh in south-east
609 England. Journal of Applied Ecology **41:** 449-463.

610 Pontee, N. 2013. Defining coastal squeeze: A discussion. Ocean & coastal
611 management **84:** 204-207.

612 Scyphers, S. B., S. P. Powers, K. L. Heck, Jr., and D. Byron. 2011. Oyster Reefs as
613 Natural Breakwaters Mitigate Shoreline Loss and Facilitate Fisheries. Plos
614 One **6:** e22396.

615 Silliman, B. R. and others 2012. Degradation and resilience in Louisiana salt marshes
616 after the BP–Deepwater Horizon oil spill. Proceedings of the National
617 Academy of Sciences **109:** 11234-11239.

618 Sistermans, P., and O. Nieuwenhuis. 2019. Western scheldt estuary (the netherlands).

619 Strong, D. R., and D. R. Ayres. 2013. Ecological and evolutionary misadventures of
620 *Spartina*. Annual Review of Ecology, Evolution, and Systematics **44:** 389-410.

621 Suykerbuyk, W. and others 2016. Surviving in changing seascapes: Sediment
622 dynamics as bottleneck for long-term seagrass presence. Ecosystems **19:** 296-
623 310.

624 Swart, D. 1977. Predictive equations regarding coastal transports, p. 1113-1132.
625 Coastal Engineering 1976.

626 Syvitski, J. P. M. and others 2009. Sinking deltas due to human activities. Nature
627 Geosci **2:** 681-686.

628 Temmerman, S., T. Bouma, J. Van de Koppel, D. Van der Wal, M. De Vries, and P.
629 Herman. 2007. Vegetation causes channel erosion in a tidal landscape.
630 Geology **35:** 631-634.

631 Temmerman, S., P. Meire, T. J. Bouma, P. M. J. Herman, T. Ysebaert, and H. J. De
632 Vriend. 2013. Ecosystem-based coastal defence in the face of global change.
633 Nature **504:** 79-83.

634 Tucker, M.J., Pitt, E.G., 2001. Waves in Ocean Engineering. Elsevier Ocean
635 Engineering. Book Series. vol. 5. Elsevier, Amsterdam.

636 van de Koppel, J., D. van der Wal, J. P. Bakker, and P. M. Herman. 2005. Self -
637 organization and vegetation collapse in salt marsh ecosystems. The American
638 Naturalist **165:** E1-E12.

639 van der Wal, D., and K. Pye. 2004. Patterns, rates and possible causes of saltmarsh
640 erosion in the Greater Thames area (UK). Geomorphology **61:** 373-391.

641 van der Wal, D., A. Wielemaker-Van den Dool, and P. M. J. Herman. 2008. Spatial
642 patterns, rates and mechanisms of saltmarsh cycles (Westerschelde, The
643 Netherlands). Estuarine Coastal and Shelf Science **76:** 357-368.

644 van Rijn, L. C. 1993. Principles of sediment transport in rivers, estuaries and coastal
645 seas. Aqua Publication.

646 van Wesenbeeck, B. K., J. van de Koppel, P. M. J. Herman, J. P. Bakker, and T. J.
647 Bouma. 2007. Biomechanical warfare in ecology; negative interactions
648 between species by habitat modification. Oikos **116:** 742-750.

649 Walling, D. E., and D. Fang. 2003. Recent trends in the suspended sediment loads of
650 the world's rivers. Global and Planetary Change **39:** 111-126.

651 Wang, H. and others 2017. Zooming in and out: Scale dependence of extrinsic and
652 intrinsic factors affecting salt marsh erosion. Journal of Geophysical Research:
653 Earth Surface **122:** 1455-1470.

654 Wolters, M., and J. P. Bakker. 2002. Soil seed bank and driftline composition along a
655 successional gradient on a temperate salt marsh. Applied Vegetation Science **5:**
656 55-62.

657 Xiao, D., L. Zhang, and Z. Zhu. 2009. A study on seed characteristics and seed bank
658 of *Spartina alterniflora* at saltmarshes in the Yangtze Estuary, China.
659 Estuarine Coastal and Shelf Science **83:** 105-110.

660 Xiao, D., L. Zhang, and Z. Zhu. 2010. The range expansion patterns of Spartina
661 alterniflora on salt marshes in the Yangtze Estuary, China. Estuarine, Coastal
662 and Shelf Science **88:** 99-104.

663 Yang, S. L. and others 2008. Spatial and temporal variations in sediment grain size in
664 tidal wetlands, Yangtze Delta: On the role of physical and biotic controls.
665 Estuarine, Coastal and Shelf Science **77:** 657-671.

666 Zhu, Z., T. J. Bouma, T. Ysebaert, L. Zhang, and P. M. J. Herman. 2014. Seed arrival
667 and persistence at the tidal mudflat: identifying key processes for pioneer
668 seedling establishment in salt marshes. Marine Ecology Progress Series **513:**
669 97-109.

670 Zhu, Z. and others 2016. Sprouting as a gardening strategy to obtain superior
671 supplementary food: evidence from a seed-caching marine worm. Ecology **97:**
672 3278-3284.

673 Zhu, Z., L. Zhang, N. Wang, C. Schwarz, and T. Ysebaert. 2012. Interactions between
674 the range expansion of saltmarsh vegetation and hydrodynamic regimes in the
675 Yangtze Estuary, China. Estuarine Coastal and Shelf Science **96:** 273-279.

676

677

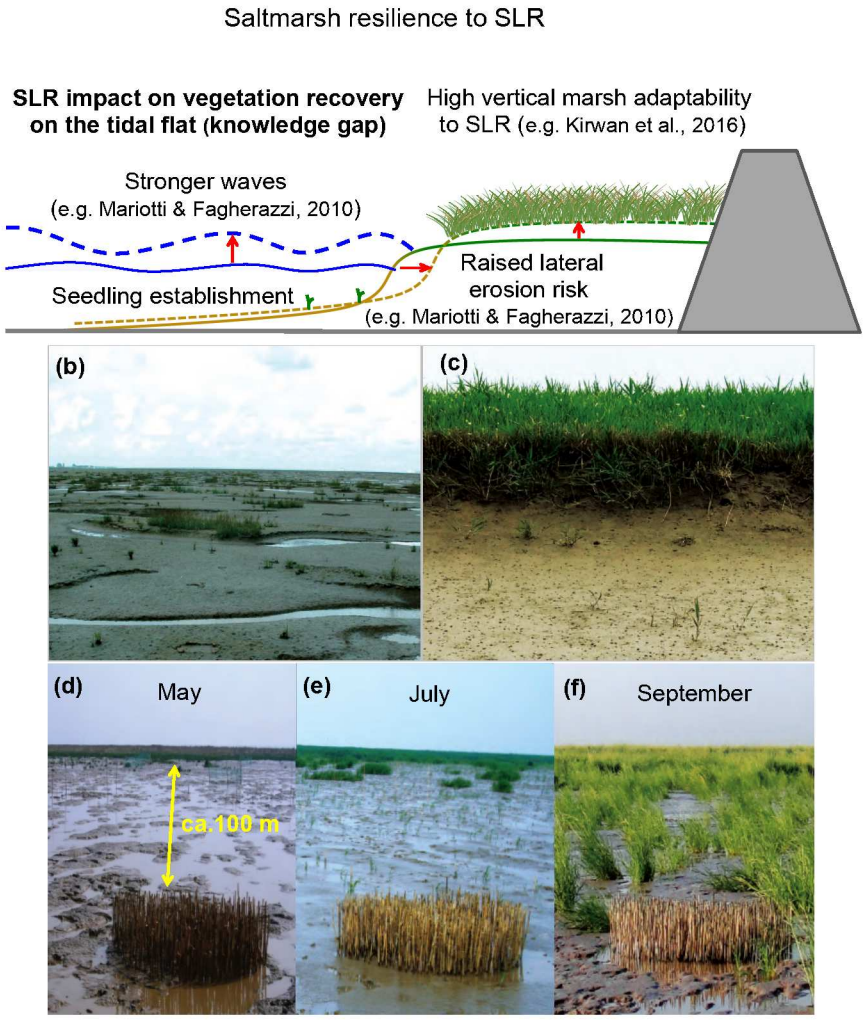

Figure.1 (a) Established knowledge and current knowledge gaps on marsh resilience to sea level rise (SLR) and increased wave action. Especially knowledge on the marsh recovery on bare tidal flats is essential for enhancing current understanding of long-term marsh resilience to SLR and associated increase in wave forcing. (b) Vegetation development in tidal flats by seedling establishment in Hooge platen, the Netherlands; (c) Seedling establishment in front of a cliff at a marsh edge in the Yangtze estuary, China; (d-f) Extensive seedling establishment of smooth cordgrass (*Spartina alterniflora*) lead to rapid vegetation expansion in a marsh in the Yangtze estuary, China.

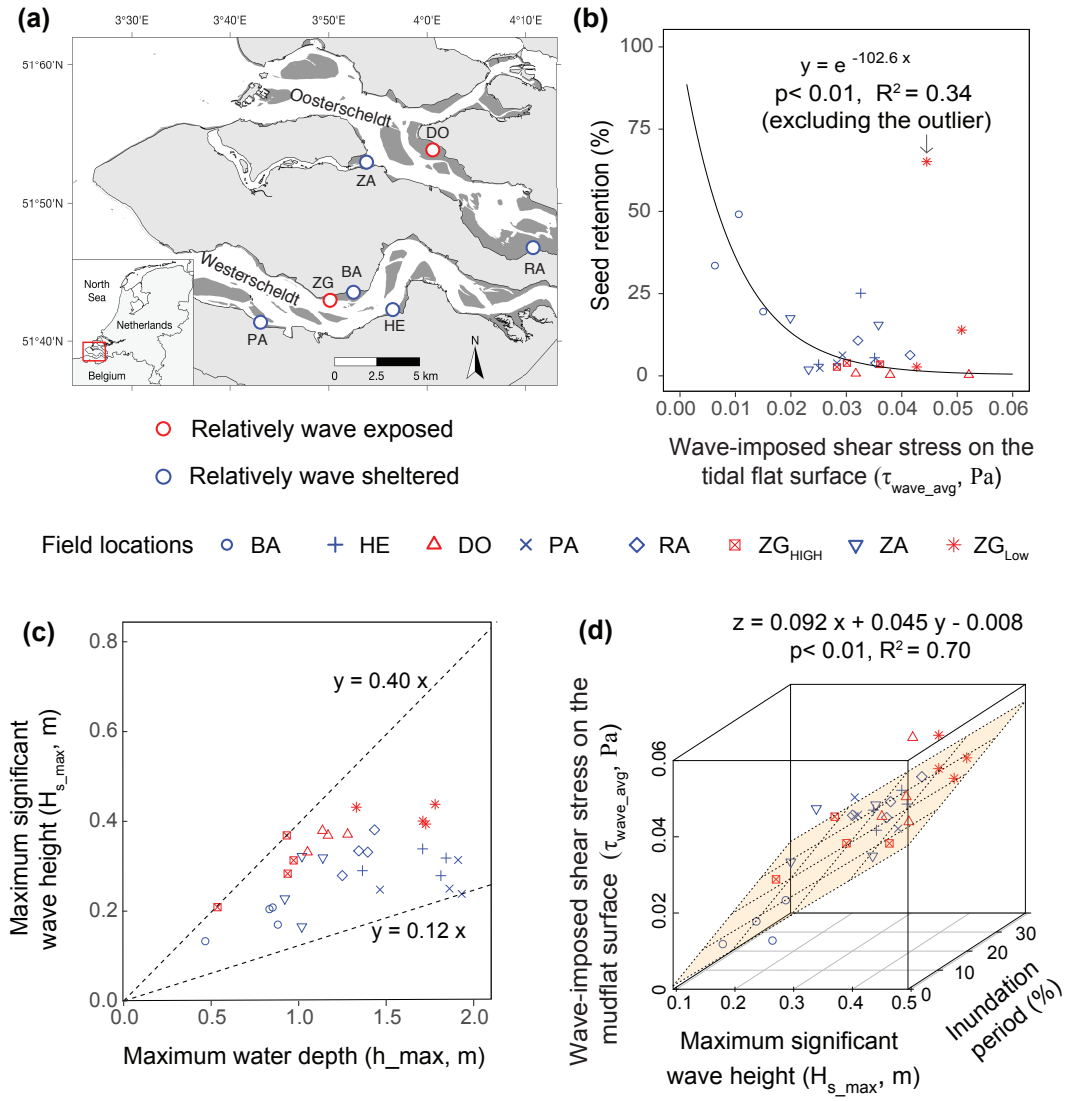

Figure. 2 (a) Geographic locations of the selected field sites; sites marked in red are relatively wave-exposed and those in blue are relatively sheltered. Site ZG includes two locations of different intertidal elevations: ZG_{HIGH} and ZG_{LOW}. Detailed site characteristics are shown in supplementary Table. 1. (b) Surface seeds retention declined exponentially with time-averaged wave-induced bed shear stress (τ_{wave_avg}). This relation was significant (Pearson's correlation, $p < 0.01$) when excluding the only outlier observed at ZG_{LOW} . (c) Observed relationship between maximum significant wave height (H_{s_max}) and maximum water depth ($h_{\_max}$). (d) Time-averaged wave-induced bed shear stress (τ_{wave_avg}) correlates positively with maximum significant wave height and inundation period (Linear model, $p < 0.001$).

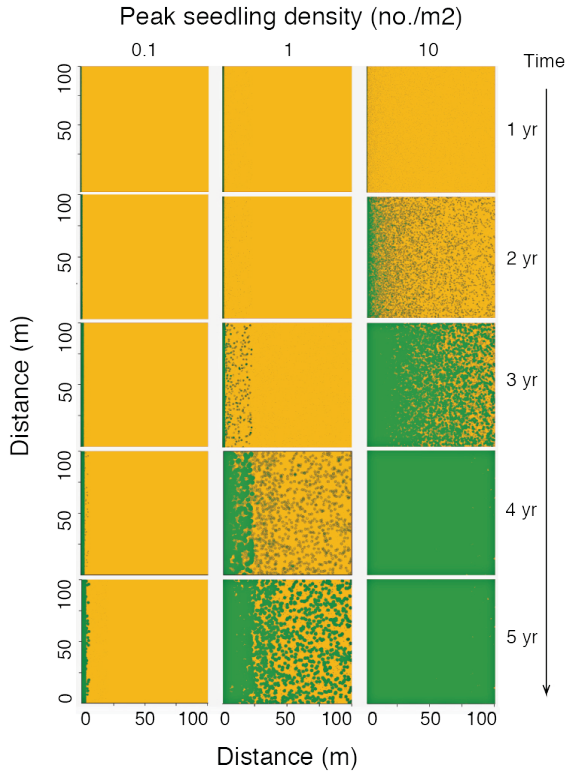

Figure. 3 Temporal dynamics of vegetation expansion/recovery on tidal flats under three different scenarios of peak seedling density. For each scenario, one typical example of vegetation expansion process within 5 years was shown. The vegetation was marked in green with the bare mudflat shown in brown.

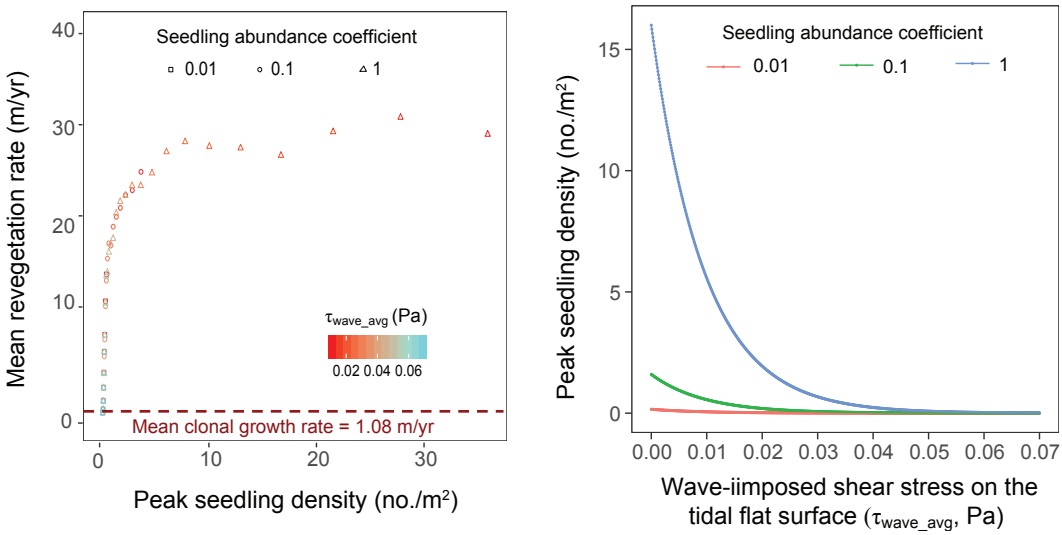

Figure. 4 (a) In the model, mean revegetation rate (m/yr) increases non-linearly with peak seedling density. Revegetation is generally much faster when seed colonization is enabled than when revegetation is achieved by only clonal growth from the existing marsh edge. Time-averaged wave-induced bed shear stress (τ_{wave_avg}) affects the revegetation rate by modifying peak seedling density. (b) Peak seedling density declined non-linearly with time-averaged wave-induced bed shear stress (τwave_avg), with its magnitude regulated by seedling abundance coefficient, a parameter that reflects the lumped effects of all factors other than waves on seedling recruitment,

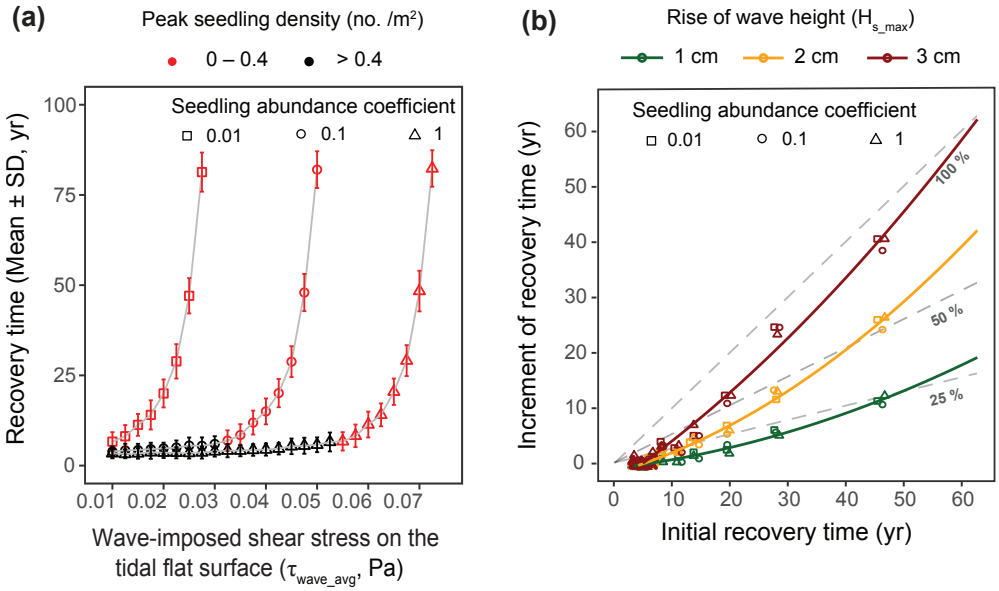

Figure. 5 (a) Modelled marsh recovery time (Mean ± SD, n = 100) grows rapidly with increasing wave-imposed shear stress on the tidal flat near the marsh edge (τ_{wave_avg}, Pa) when the peak seedling density (no./m^2) is low (0-0.4), whereas the recovery time did not change much with a high (> 0.4) peak seeding density. The sensitivity of recovery time to τ_{wave_avg} increases with decreased value of seedling abundance coefficient, i.e. stronger negative effects from other stressors. (b) The response of recovery time lengthening to small increases (1, 2 and 3 cm) of maximum significant wave height (H_{s_max}) due to the deeper water conditions on the tidal flat as result of SLR, in relation to the initial recovery time. The data points include both scenarios of peak seedling density (no./m^2), i.e.'0-0.4' and '>0.4'. Each curve fit was done with a quadratic function $y = a*x^2$, which explained best the observed increasing trend. The three dashed reference lines represent the conditions when the increment of recovery time is 25%, 50% and 100% of the initial recovery time, respectively.

Table. 1 Characteristics of field locations

Field locations		Wind exposure	Elevation (cm NAP)	Maximum water depth (m)
Oosterschelde	DO	Exposed	90	1.3
	RA	Sheltered	92	1.4
	ZA	Sheltered	85	1.1
Westerschelde	ZG_{LOW}	Exposed	89	1.8
	ZG_{HIGH}	Exposed	175	1.0
	BA	Sheltered	175	0.9
	HE	Sheltered	102	1.8
	PA	Sheltered	82	1.9

Table. S1 Time table (Year =2013) for field measurements and experiments at each location

Location	T0	T1	T2	T3	T4	T5
DO	Apr.3	May.1	May.29	Jun.18	Jul. 2	Jul.8
RA	Apr.3	May.1	May.29	Jun.18	Jul. 2	Jul.8
ZA	Apr.3	May.1	May.29	Jun.18	Jul.4	Jul.9
ZG_{LOW}	Apr.4	May.2	May.30	Jun.19	Jul. 2	Jul.10
ZG_{HIGH}	Apr.4	May.2	May.30	Jun.19	Jul. 2	Jul.10
BA	Apr.4	May.2	May.30	Jun.19	Jul. 2	Jul.9
HE	Apr.5	May.3	May.31	Jun.20	Jul.4	Jul.11
PA	Apr.5	May.3	May.31	Jun.20	Jul.4	Jul.11

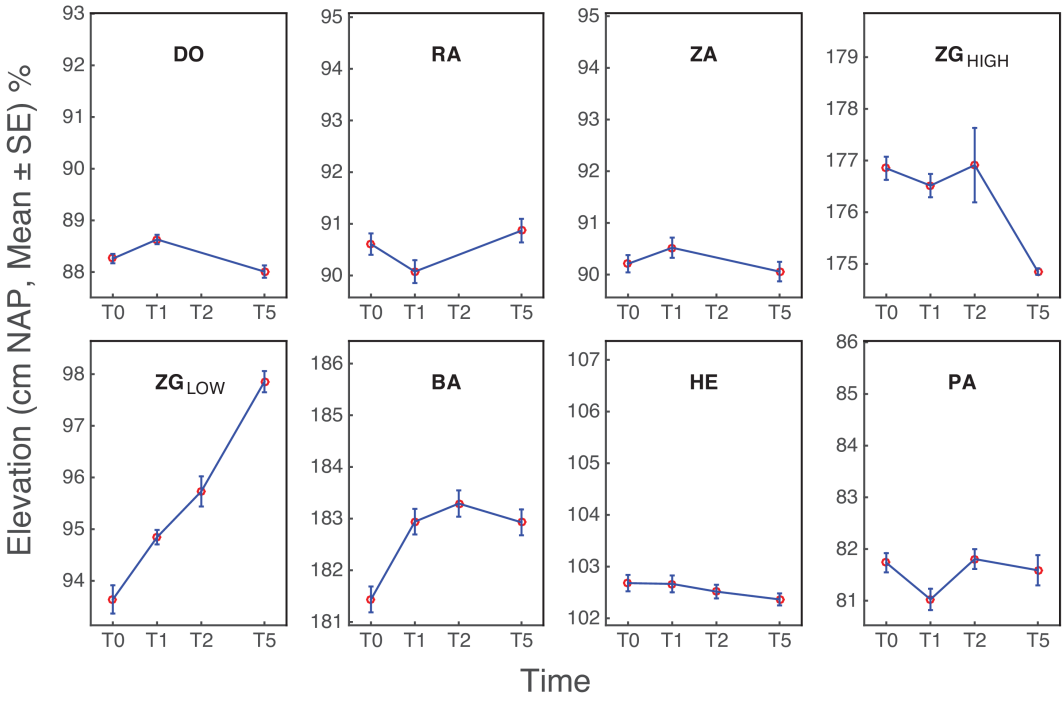

Figure. S1 Bed level changes on mudflats near the marsh of all study locations during the experiment period (T0-T5, detailed schedule shown in Table. S2), monitored using a 3D Laser scanner (RIEGL VZ-400, see methods for details).

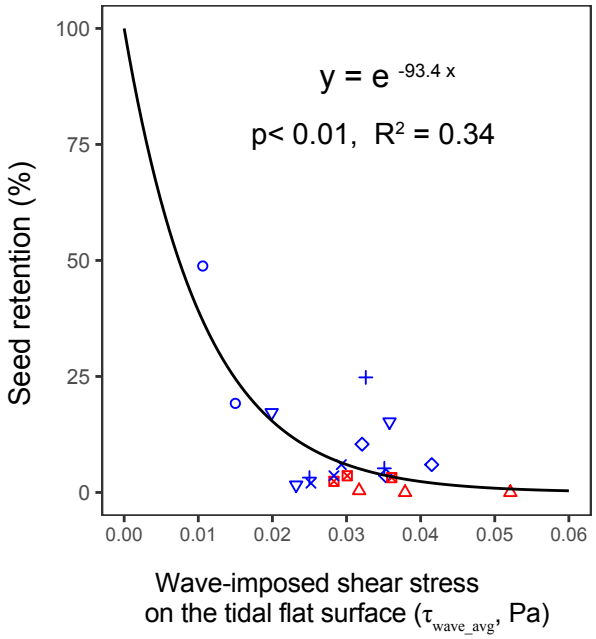

Figure. S2 Surface seeds retention declined exponentially with time-averaged wave-induced bed shear stress (τ_{wave_avg}). This relation was significant (Pearson's correlation, $p < 0.01$), when excluding all the data points associated with fast sediment accretion (greater than 1 mm/d, Fig. S1). Excluded data points: n=3 (all data points) for ZG_{LOW} and n=1 for BA (T0-T1).

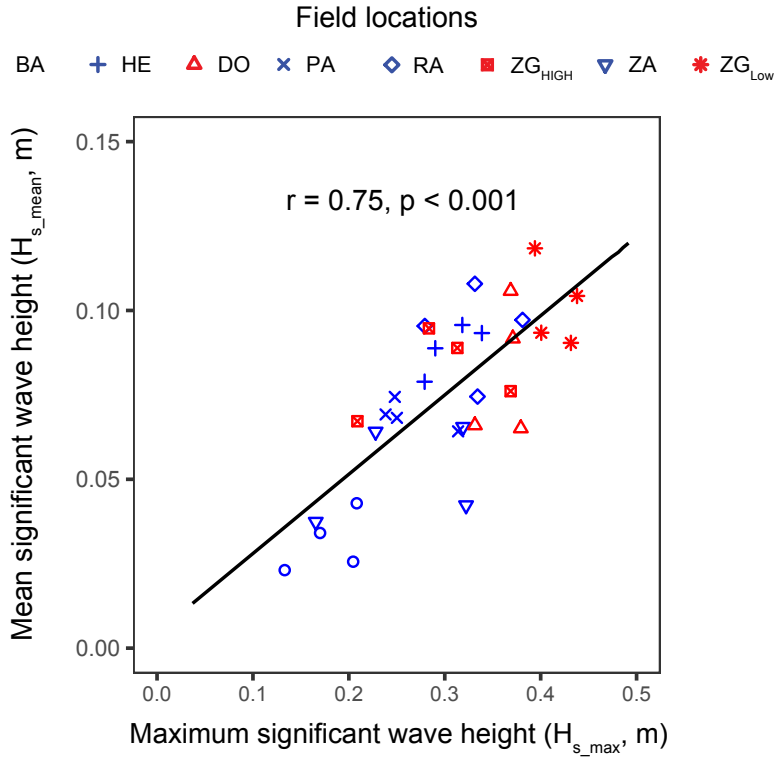

Figure. S3 A linear correlation between maximum significant wave height (H_{s_max}) and mean significant wave height (H_{s_mean}) on the mudflat near the marsh at all the study locations (Fig. 2A).